Article:
Goetzee-Barral, AJ, Usher, T-M, Stevenson, TJ et al. (4 more authors) (2017) Electric field dependent local structure of (KxNa1−x)0.5Bi0.5TiO3. Physical Review B - Condensed Matter and Materials Physics, 96 (1). 014118. ISSN 1098-0121

https://doi.org/10.1103/PhysRevB.96.014118

Electric-field-dependent local structure of $(K_x Na_{1-x})_{0.5} Bi_{0.5} TiO_3$

A.J. Goetzee-Barral[1], T.-M. Usher[2], T.J. Stevenson[1], J.L. Jones[3], I. Levin[4], A.P. Brown[1], A.J. Bell[1]

[1] School of Chemical and Process Engineering, University of Leeds, Leeds LS2 9JT, UK

[2] Chemical and Engineering Materials Division, Oak Ridge National Laboratory, Oak Ridge, Tennessee 37831, USA

[3] Department of Materials Science and Engineering, North Carolina State University, Raleigh, North Carolina 27695, USA.

[4] Materials Measurement Science Division, National Institute of Standards and Technology, Gaithersburg, Maryland 20899, USA

The in situ X-ray Pair Distribution Function (PDF) characterisation technique has been used to study the behaviour of $(K_x Na_{1-x})_{0.5} Bi_{0.5} TiO_3$, as a function of electric field. As opposed to conventional X-ray Bragg diffraction techniques, PDF is sensitive to local atomic displacements, detecting local structural changes at the Ångstrom to nanometre scale. Several field-dependent ordering mechanisms can be observed in x = 0.15, 0.18 and at the morphotropic phase boundary (MPB) composition x = 0.20. X-ray total scattering shows suppression of diffuse scattering with increasing electric field amplitude, indicative of an increase in structural ordering. Analysis of PDF peaks in the 3-4 Å range shows ordering of Bi-Ti distances parallel to the applied electric field, illustrated by peak amplitude redistribution parallel and perpendicular to the electric field vector. A transition from ‹110› to ‹112› type off-centre displacements of Bi relative to the neighbouring Ti atoms are observable with increasing x. Analysis of PDF peak shift with electric field show the effects of Bi-Ti redistribution and onset of piezoelectric lattice strain. The combination of these field-induced ordering mechanisms is consistent with local redistribution of Bi-Ti distances associated with domain reorientation and an overall increase in order of atomic displacements.

I. INTRODUCTION

Piezoelectric ceramic perovskite solid solutions based on $Na_{0.5}Bi_{0.5}TiO_3$ (NBT) have attracted considerable interest as potentially viable lead-free replacements for the currently used $Pb(Zr,Ti)O_3$ (PZT) materials [1]. Like PZT, these solid solutions exhibit a morphotropic phase boundary (MPB) in the vicinity of which enhancement of piezoelectric properties are observed [2,3]. NBT-$K_{0.5}Bi_{0.5}TiO_3$ (NBT-KBT) is one example of such lead-free MPB systems [4-6]. The crystal structure of pure NBT and its solid solutions is highly complex, showing symmetries dependent on sampling volume, therefore termed pseudosymmetries [7]. At room temperature, NBT exhibits monoclinic symmetry shown by X-ray diffraction (XRD) [8,9] previously described as rhombohedral [10,11]. Transmission electron microscopy (TEM) results indicate two modes of octahedral tilting (anti-phase and in-phase) featuring distinct coherence lengths. These modes compete with ferroelectric cation (Bi, Ti) displacements to yield a sequence of temperature dependent polymorphic phase transitions [7]. Additionally, local structure studies of NBT using neutron total scattering have suggested local Bi displacements are strongly anisotropic with their preferential directions being temperature dependent [12,13]. X-ray powder diffraction analysis of electrically poled and unpoled samples of NBT indicated that the poling process is accompanied by a phase transition from the monoclinic to rhombohedral structure [14]. This inference received support from the recent in situ studies of field-induced structural changes in NBT using X-ray total scattering measurements during application of electric field [15]. The occurrence of the monoclinic-rhombohedral transition was evidenced both by Rietveld refinements using the diffraction patterns and by analysis of the corresponding PDFs which revealed abrupt changes in the distributions of Bi-Ti bond distances, consistent with subsequent reorientation of the rhombohedral ferroelectric domains expected upon poling [15].

The solid solution between NBT and $K_{0.5}Bi_{0.5}TiO_3$ ((1-x)NBT-xKBT) exhibits the same degree of structural complexity encountered in NBT. It has attracted interest because of the MPB between rhombohedral and tetragonal phases around x = 0.20 [4-6]. Here a significant enhancement in piezoelectric properties is observed over pure NBT, increasing the d_{33} from ~65 to ~190 pC/N [16-18]. A TEM study has shown a transition across the MPB from a rhombohedral/monoclinic anti-phase tilt to short range in-phase tilts in a tetragonal phase. Additionally, the coupling between ferroelectric cation displacements and octahedral tilts

decreases with increasing x. Again, the phases are termed "pseudosymmetric" due to dependence of their symmetry on sampling volume. At the MPB both rhombohedral and tetragonal pseudosymmetries persist, also observed via X-ray diffraction [19]. Previous electric-field dependent X-ray diffraction measurements have identified significant electric-field-dependent structural transition from pseudo- to more definite tetragonal and rhombohedral symmetries [17,20].

In this study we examine local structure of NBT-KBT by X-ray total scattering techniques in situ, under electric field. This technique provides insight to the structural changes occurring from the sub-nm to the microscopic scale.

II. EXPERIMENTAL DETAILS

$(K_x Na_{1-x})_{0.5} Bi_{0.5} TiO_3$ (x = 0.15, 0.18 and 0.2) compositions were synthesized via a conventional mixed-oxide route previously detailed in Royles et al., 2010 [20]. The powders were sintered into 1 × 1 × 5 mm ceramic bars with silver electrodes deposited on two opposing long faces. X-ray total scattering data were collected at ambient temperature using beamline 11-ID-B at the Advanced Photon Source (APS), Argonne National Laboratory [21], which is dedicated to PDF measurements. An incident beam of wavelength 0.2114 Å (58.66 keV) was used with the sample to detector distance set to produce a usable Q_{max} of 23.6 $Å^{-1}$. Figure 1 shows the experimental arrangement and the electric field vector. The sample was immersed in a Fluorinert[1] (3M, USA) bath (electrically insulating liquid) in a Kapton (DuPont, USA) container. Total scattering data were collected simultaneous to the application of a static electric field. The field was increased from 0 to 4000 V/mm in steps of 250 V/mm steps and held for 5 minutes at each field amplitude. The non-sample background scattering, including that from the Kapton container and Fluorinert liquid was measured separately and subtracted from the total signal.

[1] The identification of any commercial product or trade name does not imply endorsement or recommendation by the National Institute of Standards and Technology.

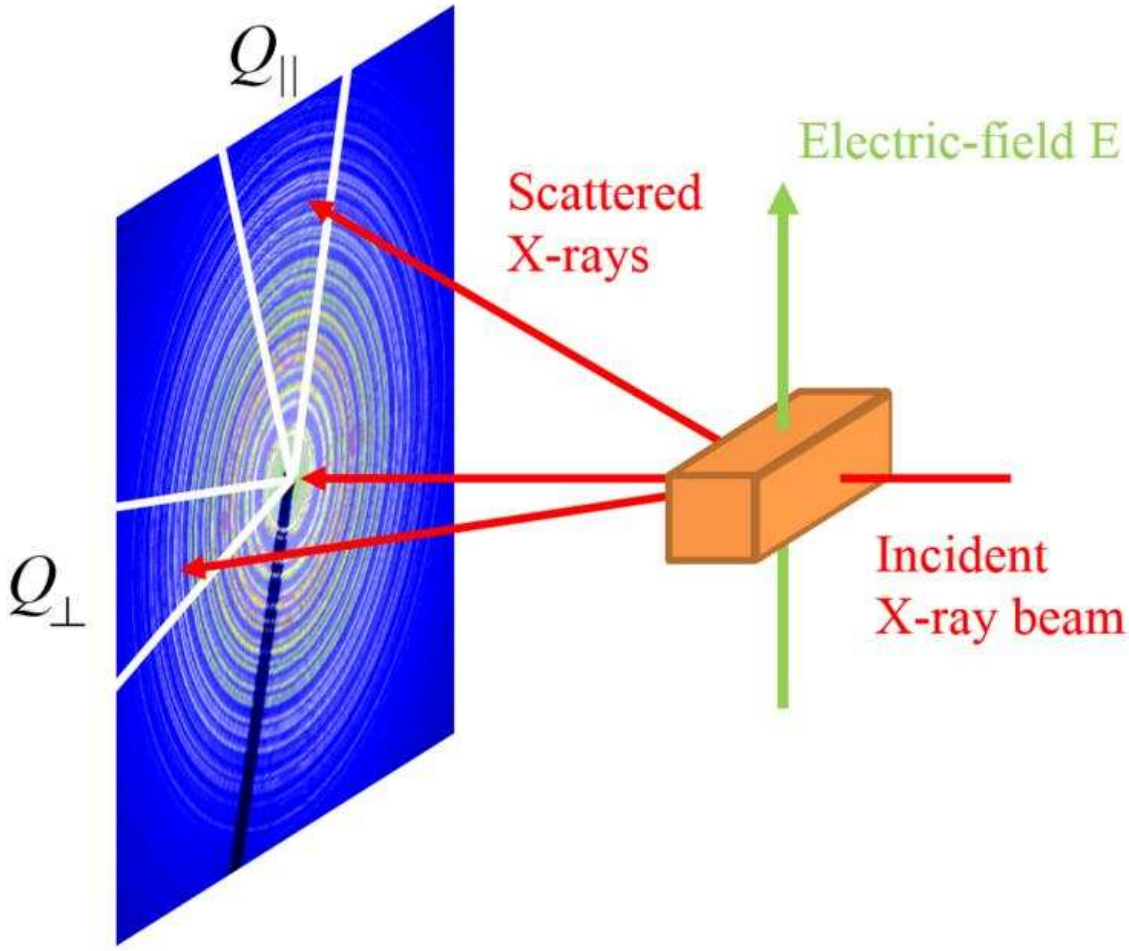

Figure 1. Schematic illustrating the X-ray scattering geometry. An electric field is applied across the sample. The scattering data for sectors parallel (‖) and perpendicular (⊥) to the electric field have been selected for this analysis.

The scattered photons were collected with a Perkin Elmer flat-panel amorphous-silicon 2D detector [21]. The software Fit2D [22] was used to process the diffraction data. Total-scattering patterns incorporating contributions from crystallites having their Q_{hkl} vectors parallel and perpendicular to the electric field were obtained by integrating ±10° sectors of the detector centred on the vertical and horizontal directions, respectively, as described in detail by Usher et al. [15]. As demonstrated previously (Usher et al, 2015), a conventional formalism involving the sine Fourier transform, as implemented in the PDFgetX3 software [23], is adequate for converting directional scattering functions, S(Q) into their corresponding directional PDFs. The PDF (G(r)) calculation is described in Equation 1.

Equation 1 $$G(r) = 4\pi r(\rho(r) - \rho_0) = \left(\frac{2}{\pi}\right)\int_{Q_{min}}^{Q_{max}} Q(S(Q) - 1)\sin(Qr)\, dQ$$

III. RESULTS AND DISCUSSION

A. Reciprocal-space data

The total-scattering pattern parallel to the electric field, $S_{\parallel}(Q)$, for x = 0.2 is shown in Figure 2, whereas the data for other compositions are included in the Supplementary Material (SM Figure 1 [24]). Similar to NBT, both $S_{\parallel}(Q)$ and $S_{\perp}(Q)$ (SM Figure 1), for all the compositions reveal suppression of diffuse scattering and sharpening of Bragg peaks with increasing electric field. These effects, which appear to be most prominent for x = 0.20, are consistent with ordering of the atomic displacements (reduced diffuse scattering), and reorientation/growth of ferroelectric domains (sharper Bragg peaks), resulting in the higher degree of overall crystallographic order in the sample. The Bragg peaks in $S_{\parallel}(Q)$ and $S_{\perp}(Q)$, shift to lower and higher Q-values, respectively, due to effects of piezoelectric strain (i.e., expansion of the lattice parallel to the direction of the field and the corresponding contraction in the perpendicular direction).

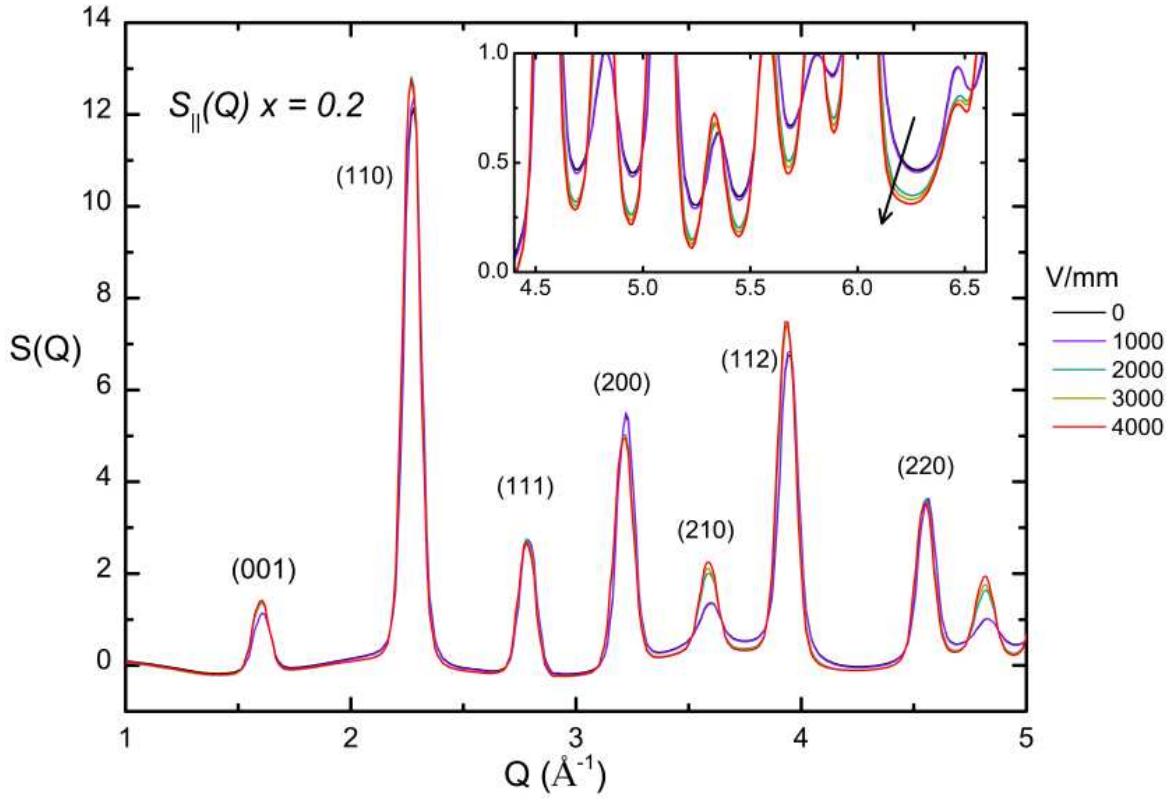

Figure 2. Total scattering structure factor $S_{\parallel}(Q)$ for x = 0.2. This composition showed the greatest magnitude of background suppression (shown in the inset) and peak sharpening.

All peaks shown also show slight shifts to lower Q (higher d-spacings) with increasing field.

B. Pair distribution function analysis

As discussed previously (Usher et al, 2015), a PDF obtained from directional total scattering, describes a distribution of all interatomic distances parallel to a given direction in the sample. Figure 3 shows $G_{\parallel}(r)$ ($G_{\perp}(r)$ shown in SM Figure 2) for all compositions for electric field, E = 0 and E = 4000 V/mm (the maximum field applied), and the difference between the two PDFs. At 4000 V/mm, the $G_{\parallel}(r)$ peaks are sharper, and this is most prevalent for x = 0.20. This reflects smaller atomic displacement parameters and stronger correlation between the atom-pairs forming the given peaks, as expected from the suppression of diffuse scattering. The MPB composition x = 0.20 has a significantly greater response to the applied field.

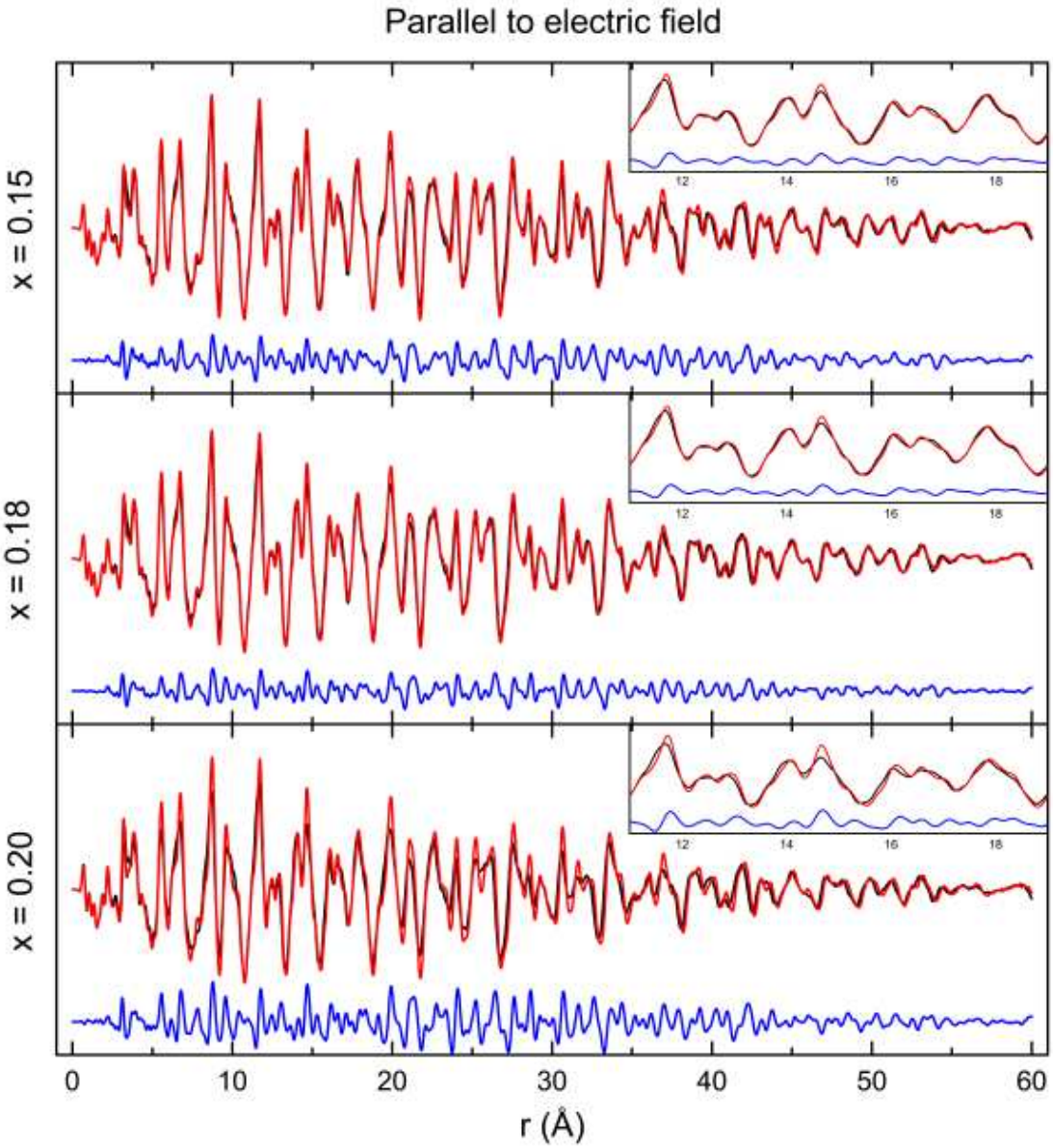

Figure 3. $G_{||}(r)$ for x = 0.15, 0.18 and 0.20 for E = 0 (black), E = 4000 V/mm (red) and the difference (blue). Inset shows the peak sharpening that is occurring across the entire range of r indicating field induced ordering and reduction in atomic displacement parameters, which account for both thermal and static displacements

Figure 4 more clearly displays low and high-r portions of the PDFs for x = 0.15-0.20 parallel and perpendicular to the field. The low-r range includes distances within the unit cell up to the cell parameter distance around 4 Å. Peaks in this region correspond to the perovskite unit cell parameter distance A-A site and B-B site in the 3.9 – 4 Å region, and A-B site distances pin the 3.2 – 3.8 Å region. The approximate positions of peaks at this range are highlighted by vertical black tick marks. The high-r portion of the PDF shows distances at greater length-scales

> 40 Å. It is apparent that under an electric field, two distinct phenomena are taking place. Parallel to the electric field vector the high-r distances extend in r, attributed to piezoelectric lattice strain. The opposite behaviour is observed perpendicular to the field. The lattice contracts in order to accommodate the anisotropic strain. The low-r behaviour opposes the high-r peak shifts by contraction and extension of peak positions parallel and perpendicular to the field vector respectively. In the following sections this apparent disparity between the ranges will be examined. Analysis of the low-r peak behaviour demonstrates that the apparent converse shift is a result of the redistribution of Bi-Ti distances with electric field, giving the impression of peak shifting behaviour, whilst high-r analysis demonstrates the longer scale field induced strain behaviour.

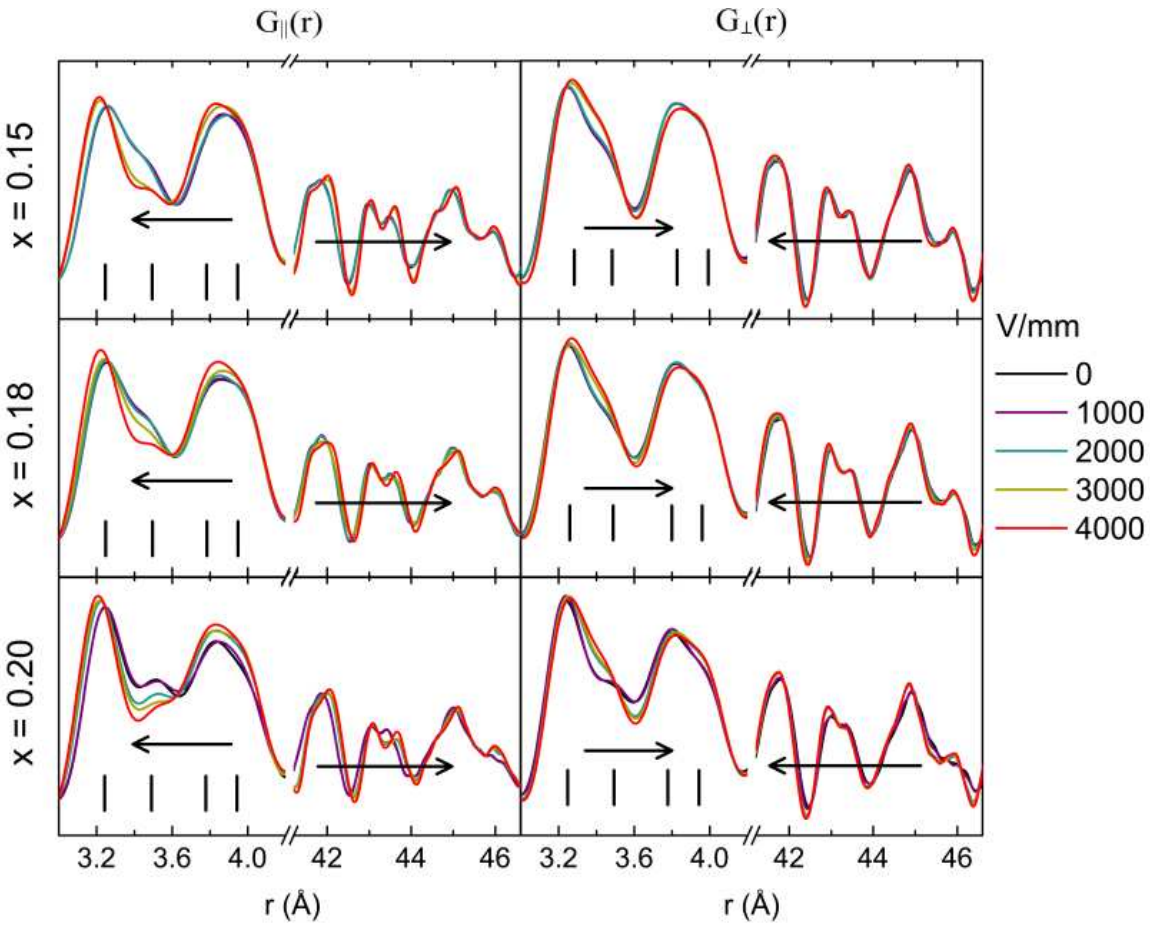

Figure 4. Low and high r G(r) as a function of field for $G_{||}(r)$ (parallel) and $G_{\perp}(r)$ (perpendicular) for x = 0.15, 0.18 & 0.2. The four peaks in the low r region are highlighted

by black vertical tick marks. High-r peaks shift to higher and lower r for $G_{||}(r)$ and $G_{\perp}(r)$, respectively.

1. Low r peak analysis

Peak fitting was used to study the behaviour of low r PDF peaks, similar to the analysis performed previously by Usher et al. for NBT. As in NBT, an X-ray PDF of NBT-KBT emphasizes interatomic distances involving Bi, which provides a dominant contribution to the total-scattering signal. The intrinsically weak nearest-neighbour Ti-O peak (around 1.95 Å) is further obscured by oscillations resulting from the relatively limited Q_{max} value used in the Fourier transform of the total-scattering function.

Therefore, our analysis focused on the peaks around 3.5±0.3 Å (Bi-Ti distances) and around 4 Å (Bi-Bi, Ti-Ti, plus all other distances at this lattice-parameter spacing). There are atom-pair distances within the unit cell up to 7 Å, however above 4 Å multiple atom pairs contribute single peaks, which would be non trivial to separate in order to form a displacement model. The off centering of Bi with respect to Ti produces a splitting of Bi-Ti distances where the shortest Bi-Ti distance is around 3.2 Å showing good agreement with EXAFS measurements [25]. There is some contribution from the longest Bi-O distances that arise in the case of a rhombohedral structure (SM Figure 3), though its effect is small and distributed between more than one Bi-Ti distance, thereby reducing its impact.

The radial distribution function (RDF) G*(r) can be obtained from the PDF, shown in Equation 3, where ρ_0 is the number density. The area under a RDF peak at a distance r is proportional to the multiplicity of that particular interatomic distance [26]. By determining the ratios of the areas of the various Bi-Ti peaks, the relative coordination number can be calculated for a specific atom-pair distance and therefore the effective Bi^{3+} displacement direction within a pseudocubic unit cell can be inferred.

Equation 3
$$G^*(r) = \big(G(r) + (4\pi r\rho_0)\big)r$$

Table 1 and Figure 5 illustrate the splitting of Bi-Ti bond distances arising from 3 common ferroelectric displacement directions. The distances have been labelled short,

intermediate and long, or R1, R2, and R3, respectively. Table 1 includes the ‹112› displacement, which approximates to a 3:2:3 R1:R2:R3 ratio. The ‹112› displacements can also be interpreted as effective averages of displacements occurring along higher-symmetry crystallographic directions. One such averaging scenario could involve a combination of the local ‹111› and ‹001› Bi shifts in the coexisting rhombohedral and tetragonal domains, respectively, while another could relate to a combination of ‹101› and ‹011› displacements in different locally monoclinic/orthorhombic domains.

Table 1. Ideal area ratios for the peaks associated with the split distances arising from various central ion (Bi-Ti) displacement directions.

Displacement direction	Short: R1	Intermediate: R2	Long: R3
‹001›	4	-	4
‹111›	1	6	1
‹110›	2	4	2
‹112›	3	2	3

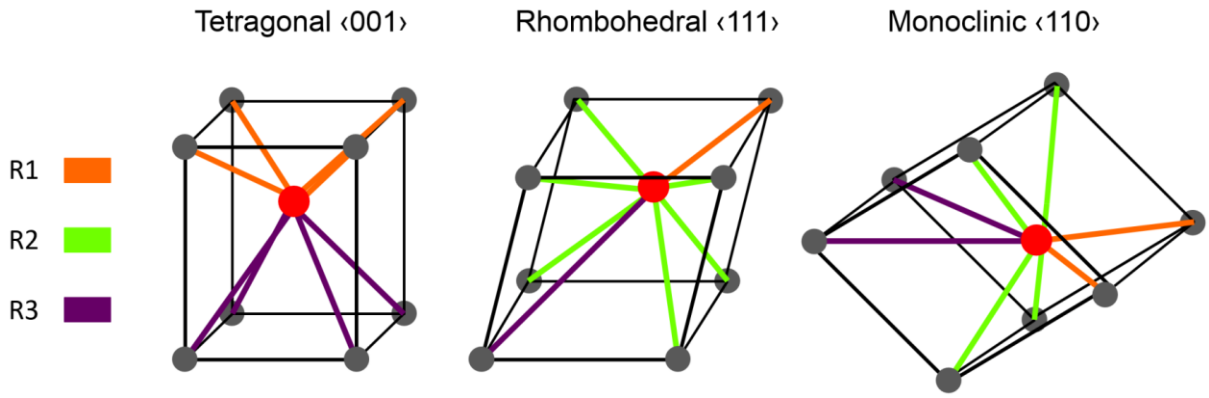

Figure 5. Schematic illustrating the various atom-atom distances in idealised non-centrosymmetric structures with exaggerated distortions. The Bi^{3+} central ion is coordinated by 8 Ti^{4+} ions.

Figure 6 shows the G*(r) 0-field data to which the ‹110› and ‹112› displacement models have been applied. Models for tetragonal ‹001› and rhombohedral ‹111› displacements

produced extremely poor fits and are therefore not considered. The fits were done using a least-squares method and the goodness of fit (χ^2) was used to determine the best-fitting models.

The peak areas R1, R2 and R3 were constrained in their relevant ratios, and the Bi-Bi/Ti-Ti peak area was set to a ratio of 6, as fixed by the structure. As a non-cubic structure, several atom-pair distances are expected to contribute to the Bi-Bi/Ti-Ti peak. For example a tetragonal structure would require two separate peaks and an orthorhombic would require three, however these distortions are relatively small and instead produce a broad peak. As shown in Table 2, x = 0.15 has a preferential ‹110› fit and x = 0.20 a ‹112› fit. For x = 0.18 the difference between the χ^2 values for ‹110› and ‹112› is not sufficiently distinct to differentiate between the displacement models. This suggests a gradual transition from ‹110› to ‹112› displacements as the composition approaches the MPB. Away from the MPB, rhombohedral and tetragonal fits were suitable for x = 0.10 and 0.30 respectively (SM Figure 4). This indicates a growing complexity in the local displacements as the MPB is approached.

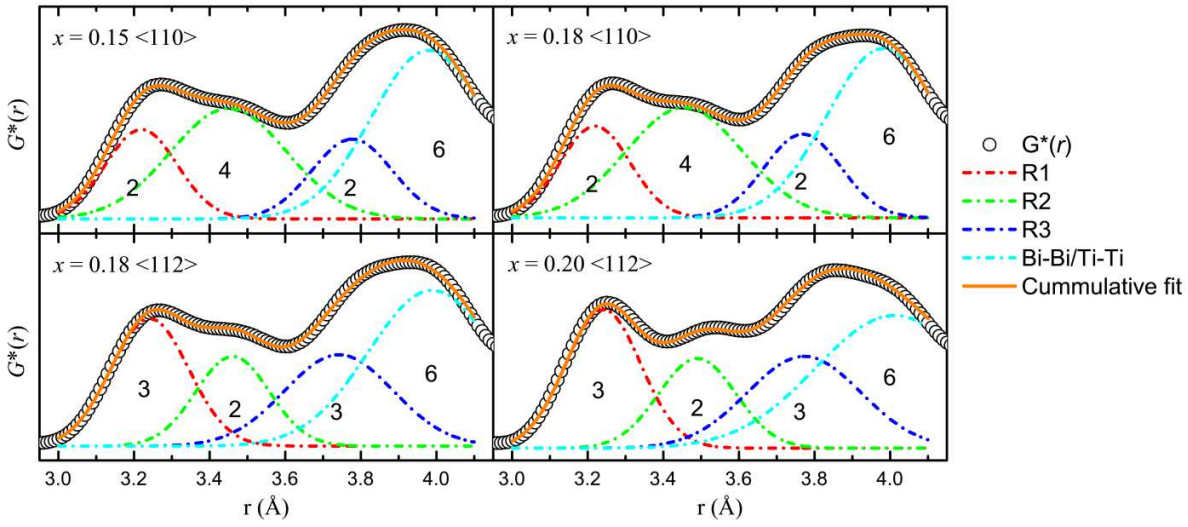

Figure 6 Bi-Ti displacement direction models (dashed lines) applied to 0-field G*(r) RDFs (white circles). Peaks are labelled with area ratios corresponding to the applied directional model.

Table 2. Goodness of fit for ‹110› and ‹112› displacement models applied to 0-field data. x = 0.15 shows a preferential ‹110› fit, whilst x = 0.20 shows a preferential ‹112› fit. For x =

0.18 the difference in fitting between the two models is relatively small and distinguishing between both is not possible A transition between ‹110› and ‹112› with increasing x is therefore suggested.

Goodness of fit: reduced χ^2			
Composition x =	<110>	<112>	Difference
0.15	0.008	0.385	0.377
0.18	0.008	0.025	0.017
0.20	0.119	0.023	0.096

The behaviour of the PDFs and the constituent peaks used to fit them (R1, R2, R3, and Bi-Bi/Ti-Ti) are shown in Figure 7 at the maximum field of 4000 V/mm. In order to observe the changing peak behaviour the area ratio constraints were removed. For all compositions there is a general increase in the contribution of R1 and R3 parallel to the electric field. In the perpendicular direction there is significant increase in the proportion of R2 and almost complete suppression of R3, which results in a greater contribution from the Bi-Bi/Ti-Ti peak.

This suggests that the Bi^{3+} cation displacements orient parallel to the electric field relative to the surrounding Ti^{4+} cations, as now more of the short and long Bi-Ti distances (R1, R3) are observed parallel to the field while more of the intermediate distances (R2) are observed perpendicular to the field. Since the relative area of the peak corresponds to the coordination number at a particular distance it is possible to infer this orientation behaviour. An example of complete redistribution is schematically depicted in Figure 8. The final displacement direction for every composition cannot be readily determined, however the shift to lower r of R2 in the perpendicular direction also suggests a final displacement approaching monoclinic. The remaining presence of R2 parallel to the field rules out a transition to a pure rhombohedral phase as was observed for NBT [15], or pure tetragonal, which for both examples would be observed as a lack of R2 altogether. These higher symmetry phases may be observable under greater electric fields.

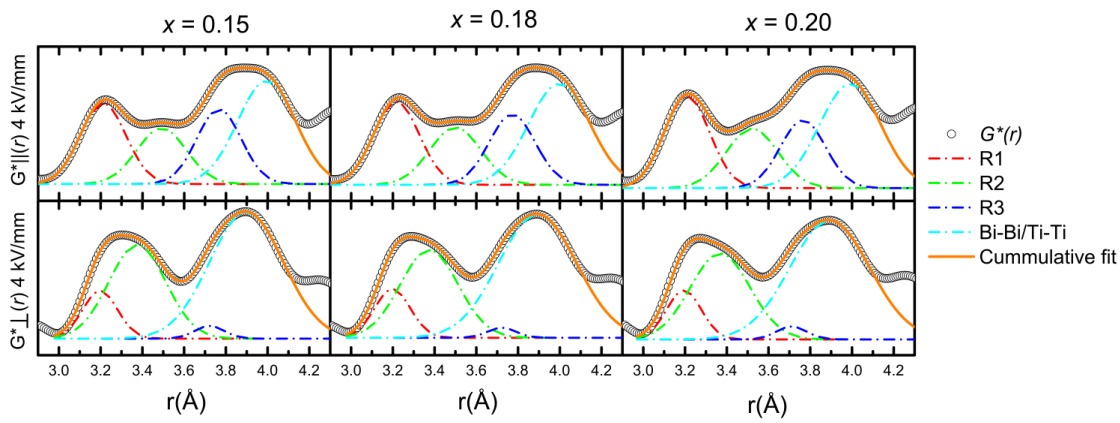

Figure 7 RDF for compositions x = 0.15, 0.18 and 0.20 at E = 4000 V/mm, parallel and perpendicular to the field. Generally parallel to the field contribution from R1 and R3 increases. Perpendicular to the field, the proportion of R2 increases significantly.

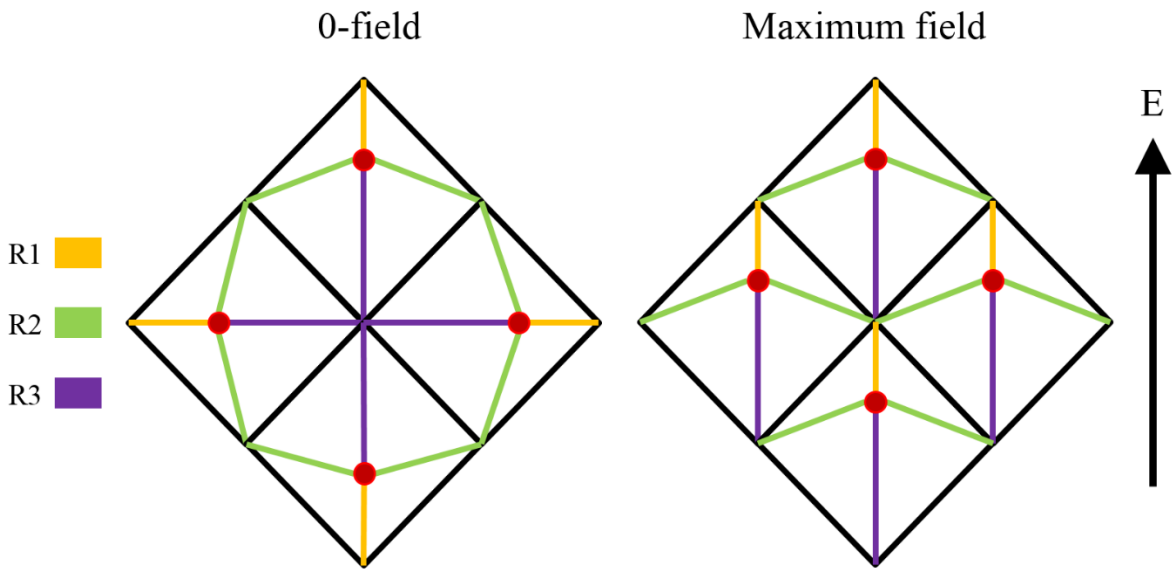

Figure 8 Idealised redistribution of Bi-Ti distances under an electric field. From an initial disordered state of Bi-Ti distributions, an electric field aligns Bi with respect to Ti. This increases the presence of R1 and R3 parallel to the electric field whilst reducing the R2 contribution, becoming more prominent perpendicular to the field.

2. Piezoelectric lattice strain

To study the high r we used an approach previously described [27] to determine the effects of electric field on PDF peak positions and changes in broadening and shape. Shown in

Equation 2, R_Δ represents the residual between the E = 0 and E = x where x is non-zero electric field, and Δ is the sampling range. R_Δ is calculated over the sampling range for E = x data shifted $\pm\delta r$ relative to E = 0, and N is the number of steps per sampling range over which the summation is performed. The value of δr, which produces the lowest R_Δ within the sampling range Δ, is then obtained. The resultant δr describes how the peaks shift and R_Δ how the shape varies with distance r under an electric field. Here, sampling ranges of 5 Å (Figure 9) are used to describe the dependence of the peak shift and residual as a function of r and E. The residual R_Δ (SM Figure 5), does not change significantly across r, although a slight positive trend is apparent, indicating high r peaks experience a greater change in shape and/or broadening than low r peaks.

Figure 9 shows δr plots for $Q_{\parallel}$ and $Q_{\perp}$. As expected from piezoelectric lattice strain effects, atom-pair distances extend parallel to the electric field, shown by the higher δr values. Conversely, transverse to the field contraction of atom-pair distances occurs as the crystal lattice accommodates the anisotropic strain. At low fields there is a relatively constant strain across r, meaning that at high r the strain is lower than expected. At greater fields this response approximates a linear trend, characteristic of classic piezoelectric strain effects. This suggests the initial low-field responses are short ranged and not correlated, becoming macroscopic at greater fields. The magnitude of the strain effects is greatest for x = 0.20 and reflects the field dependent changes observed in the PDFs. At distances below 7 Å, i.e. atom-pair distances within the unit-cell, δr crosses zero and becomes negative parallel to the electric field and positive transverse to the electric field vector, respectively. Here the low-r behaviour previously described is revealed. Above 40 Å the small PDF signal becomes very small, creating artefacts in the peak shift calculation. This issue is magnified at low fields where the relatively small peak shifts also contribute to the artefacts.

Equation 2

$$R_{\Delta} = \frac{\sum_{r}^{r+\Delta} |G(r \pm \delta r)_{E=0} - G(r)_{E=x}|}{\sum_{r}^{r+\Delta} |G(r)_{E=0}| / N}$$

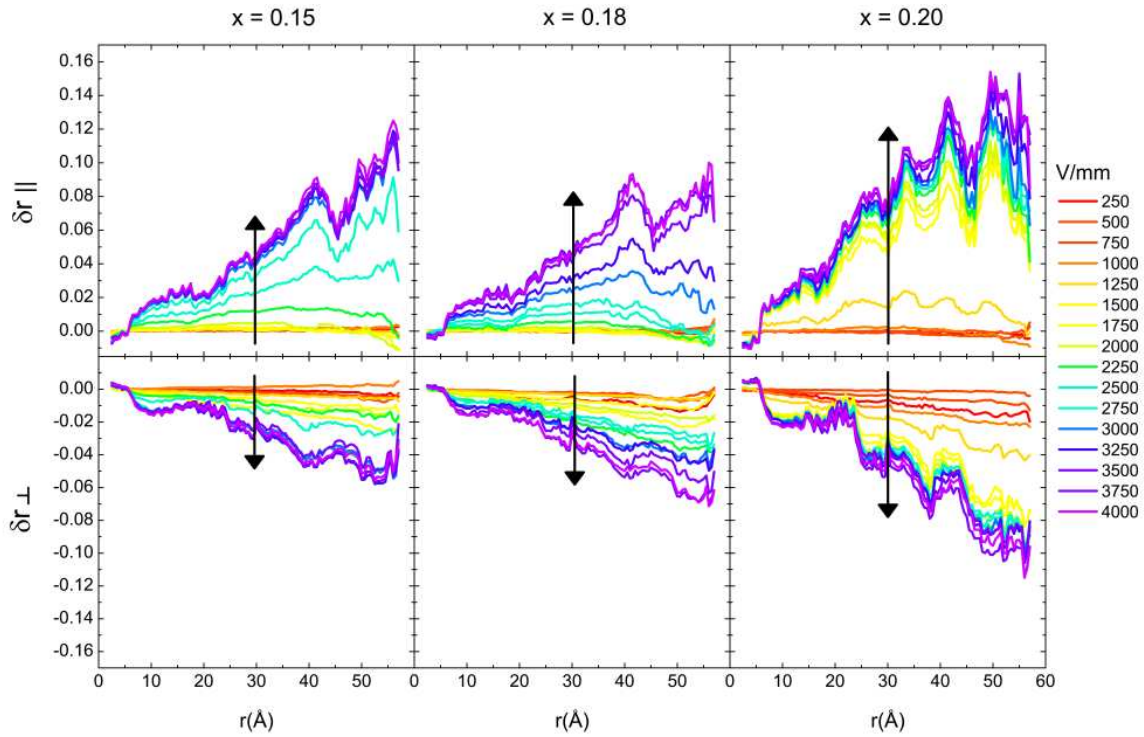

Figure 9 δr, or PDF peak shifts parallel and perpendicular to the field across r for electric fields ranging from 0 - 4000 V/mm. Arrows indicate increasing electric field.

Field-induced strain was estimated from the gradient of δr(r) using a linear regression over the 10 - 40 Å range of Figure 9, shown in Figure 10. This range was chosen as it predominantly reflects piezoelectric lattice strain. Below 10 Å low-r effects occurring at unit cell length scales begin to emerge. As previously discussed, above 40 Å artefacts of the peak shift calculation become prominent due to the small PDF amplitude above those distances. The dependence of this strain on electric field is shown in Fig. 5. Three distinct regions are observed for x = 0.20: 1) A low field region where relatively no strain is observed from 0-1000 V/mm, 2) a more rapid increase in the 1000-1500 V/mm range. At these fields diffraction experiments have shown a pseudocubic to tetragonal phase transformation [20], described as growth of tetragonal domains. This phase transition could be inferred from the sudden increase in strain, however an explicit transition to a tetragonal phase does not occur due to the remaining contribution of R2 in the RDF (Figure 7). This is followed by 3), where a linear increase is apparent, indicating piezoelectric lattice strain. x = 0.15 and 0.18 display less abrupt and lower magnitude strain responses beginning around 2250 V/mm, which plateau after 3000 - 3500

V/mm. The perpendicular strain response results in a contraction of atomic distances, due to the crystal lattice accommodating the anisotropic field, and has roughly half the magnitude of the parallel strain values.

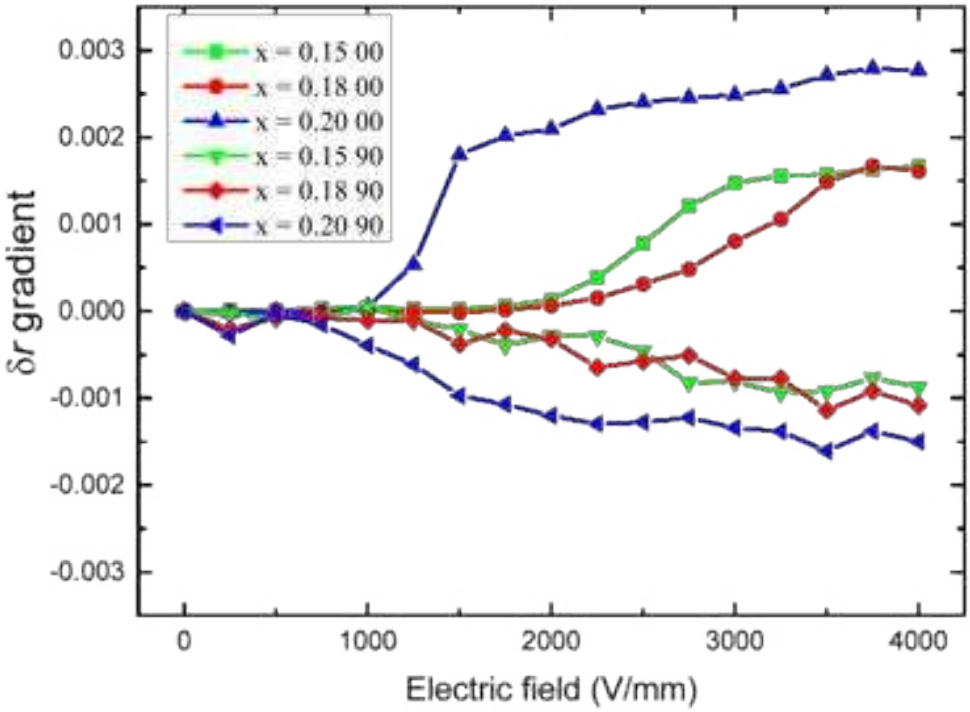

Figure 10. Gradient of δr(r) which is equivalent to strain, parallel (00) and perpendicular (90) to the electric field for x = 0.15 – 0.20.

IV. CONCLUSIONS

The local off-centre displacements of Bi relative to the nearest Ti atoms in $(K_x Na_{1-x})_{0.5} Bi_{0.5} TiO_3$ solid solutions with x = 0.15, 0.18 and 0.20 have been analysed as a function of electric field using an atomic pair-distribution function derived from X-ray total scattering.

Three Bi-Ti distances are observed: short (R1), intermediate (R2) and long (R3). When the electric field is applied, R1 and R3 appear to generally dominate parallel to the field vector whereas R2 becomes the predominant distance transverse to the field. This suggests a redistribution of Bi-Ti distances as a result of a Bi displacement relative to Ti. This appears to cause electric field induced strain evidenced from PDF peak shifts. The MPB composition displays an abrupt onset of reorientation and highest magnitude of piezoelectric lattice strain. The onset for $x < 0.20$ is less abrupt and the distinction between domain reorientation and piezoelectric lattice strain is not as clear. Across all compositions local scale strain does not initially follow a linear trend associated with ideal piezoelectric behaviour i.e. we observe non-zero but constant strain response across r. This would suggest an initial locally correlated strain, becoming macroscopic at greater fields. The previously reported phase transition observed for x = 0.20 can therefore be explained as a macroscopic phenomenon mediated by the local collective reorientation of Bi displacements induced by an applied field.

At zero field, the effective directions of Bi displacements change from ‹110› to ‹112› with x increasing from 0.15 to 0.20. This picture contrasts with NBT in which Bi atoms are locally off-centred approximately along ‹111› directions. As previously discussed the ‹112› displacement can be interpreted either as an intrinsic displacement or as an effective average of displacements occurring along other crystallographic directions, e.g., ‹111› and ‹001› Bi shifts from coexisting rhombohedral and tetragonal domains respectively, or ‹101› and ‹011› displacements from local monoclinic/orthorhombic domains. We favour this last interpretation due to the pseudosymmetric nature of the NBT-KBT system wherein the rhombohedral and tetragonal phases locally display orthorhombic or lower symmetries [19]. The number of coexisting Bi displacement directions is expected to be the largest at the MBP, which appears to promote reorientation/ordering under an electric field that is manifested in the enhanced piezoelectric properties observed for this composition.

Acknowledgements

A.J.G.-B. acknowledges funding and financial support from the Engineering and Physical Sciences Research Council and School of Chemical and Process Engineering at the University of Leeds. T.-M.U. and J.L.J. acknowledge support from the U.S. Department of Commerce under award number 70NANB13H197. This research used resources of the Advanced Photon Source, a U.S. Department of Energy (DOE) Office of Science User Facility operated for the DOE Office of Science by Argonne National Laboratory under Contract No. DE-AC02-06CH11357. The authors acknowledge Giovanni Esteves and Alexandra Henriques for their assistance during the synchrotron experiment and beamline staff: Olaf Borkiewicz, Kevin Beyer, Karena Chapman and Peter Chupas are also thanked for their assistance.

References

[1] J. Rödel, K. G. Webber, R. Dittmer, W. Jo, M. Kimura, and D. Damjanovic, J. Eur. Ceram. Soc. 35, 1659 (2015).
[2] B. Jaffe, W. R. Cook, and H. Jaffe, Piezoelectric Ceramics (Academic Press, London, 1971).
[3] A. J. Bell, J. Eur. Ceram. Soc. 28, 1307 (2008).
[4] I. P. Pronin, N. N. Parfenova, N. V. Zaitseva, V. A. Isupov, and G. A. Smolenskii, Fiz. Tverd. Tela 24, 1860 (1982).
[5] G. A. Smolenskii, V. A. Isupov, A. I. Agranovskaya, and N. N. Krainik, Sov. Phys.-Solid State 2, 2651 (1961).
[6] S. B. Vakhrushev, V. A. Isupov, B. E. Kvyatkovsky, N. M. Okuneva, I. P. Pronin, G. A. Smolensky, and P. P. Syrnikov, Ferroelectrics 63, 153 (1985).
[7] I. Levin and I. M. Reaney, Adv. Funct. Mater. 22, 3445 (2012).
[8] S. Gorfman and P. A. Thomas, J. Appl. Crystallogr. 43, 1409 (2010).
[9] E. Aksel, J. S. Forrester, J. L. Jones, P. A. Thomas, K. Page, and M. R. Suchomel, Appl. Phys. Lett. 98, 152901 (2011).
[10] I. P. Pronin, P. P. Syrnikov, V. A. Isupov, V. M. Egorov, and N. V. Zaitseva, Ferroelectrics 25, 395 (1980).
[11] G. O. Jones and P. A. Thomas, Acta Crystallogr. Sect. B-Struct. Sci. 58, 168 (2002).
[12] E. Aksel, J. S. Forrester, J. C. Nino, K. Page, D. P. Shoemaker, and J. L. Jones, Phys. Rev. B 87, 104113 (2013).
[13] D. S. Keeble, E. R. Barney, D. A. Keen,M. G. Tucker, J. Kreisel, and P. A. Thomas, Adv. Funct. Mater. 23, 185 (2013).
[14] B. N. Rao and R. Ranjan, Phys. Rev. B 86, 134103 (2012).
[15] T.-M. Usher, I. Levin, J. E. Daniels, and J. L. Jones, Sci. Rep. 5, 14678 (2015).
[16] A. Moosavi, M. A. Bahrevar, A. R. Aghaei, P. Ramos, M. Algueró, and H. Amorín, J. Phys. D 47, 055304 (2014).
[17] M. Otoničar, S. D. Škapin, M. Spreitzer, and D. Suvorov, J. Eur. Ceram. Soc. 30, 971 (2010).
[18] T. Takenaka, H. Nagata, and Y. Hiruma, IEEE Trans. Ultrason. Ferroelectr. Freq. Control 56, 1595 (2009).

[19] I. Levin, I. M. Reaney, E.-M. Anton,W. Jo, J. Rödel, J. Pokorny, L. Schmitt, H.-J. Kleebe, M. A. Hinterstein, and J. L. Jones, Phys. Rev. B 87, 024113 (2013).
[20] A. J. Royles, A. J. Bell, A. P. Jephcoat, A. K. Kleppe, S. J.Milne, and T. P. Comyn, Appl. Phys. Lett. 97, 132909 (2010).
[21] P. J. Chupas, K.W. Chapman, and P. L. Lee, J. Appl. Crystallogr. 40, 463 (2007).
[22] A. P. Hammersley, S. O. Svensson, M. Hanfland, A. N. Fitch, and D. Hausermann, High Pressure Res. 14, 235 (1996).
[23] P. Juhas, T. Davis, C. L. Farrow, and S. J. L. Billinge, J. Appl. Crystallogr. 46, 560 (2013).
[24] See Supplemental Material at http://link.aps.org/supplemental/10.1103/PhysRevB.96.014118 for figures showing additional data, displacement models for other compositions away from the MPB, and as a reference, unsuitable modes.
[25] V. A. Shuvaeva, D. Zekria, A. M. Glazer, Q. Jiang, S. M.Weber, P. Bhattacharya, and P. A. Thomas, Phys. Rev. B 71, 174114 (2005).
[26] T. Egami and S. J. L. Billinge, in Underneath the Bragg Peaks: Structural Analysis of Complex Materials, 2nd ed., edited by R. W. Kahn (Elsevier, Amsterdam, 2012), p. 1.
[27] I. Levin,V. Krayzman, J.C.Woicik, F. Bridges, G. E. Sterbinsky,
T. M. Usher, J. L. Jones, and D. Torrejon, Phys. Rev. B 93, 104106 (2016).